Pattern dynamics of the Bénard-Marangoni instability in a medium aspect ratio container

P Cerisier [1], S Rahal [2] and H Azuma [3]

[1] IUSTI - CNRS UMR 6595, Polytech'Marseille, Technopôle de Château-Gombert, 5 rue Enrico Fermi, 13453, Marseille Cedex 13, FRANCE.

[2] Department of Mechanical Engineering, University of Batna, Rue Boukhlouf Mohamed el Hadi, 05000 Batna, ALGERIA.

[3] Department of Aerospace Engineering, Osaka Prefecture University, Gakuen-cho 1-1, Sakai, Osaka 599-8531, JAPAN.

Abstract. This study is an experimental work devoted to Bénard-Marangoni instability in a medium vessel. The free surface deformation is visualised by interferometry and the free surface temperature field by infrared thermography. These two techniques are complementary, since each method provides specific information, which may allow the detection of peculiar phenomena such as the spatial resonance, which is a situation in which the interfacial deformation does not conform to the flow pattern. The influences of the aspect ratio, Rayleigh, Biot and Prandtl numbers, are considered. More dynamics are induced by increasing the Biot number. Conversely, increasing the Prandtl number reduces the dynamics. The deformation magnitude and the wavenumber increase as functions of the gradient of temperature. Two behaviours of the deformation, as a function of Prandtl and Biot numbers, were observed, depending on the value of the applied gradient of temperature. The obtained results are discussed with previous experimental, theoretical and numerical studies. Results of other authors were confirmed concerning the evolution as functions of the gradient of temperature and the aspect ratio and new results were obtained concerning the behaviour of the pattern as functions of Pr and Biot numbers.

1. Introduction

When a fluid layer is heated from below and cooled from above, beyond a critical gradient of temperature, a convection pattern is observed. In Bénard-Marangoni (BM) convection, both buoyancy and surface tension effects are involved, and beyond the onset of convection, polygonal cells are formed.

The BM convection is now widely recognized for its practical importance, due to the fact that it is omnipresent in a large variety of processes, such as crystal growth experiments, film coating processes, and low gravity fluid experiments. Many experimental studies have been carried out to study i) the onset of convection, ii) the pattern formation and dynamics, iii) the wavenumber selection, iv) the problems of disorder, etc…

For a comprehensive introduction and a review of the experimental works carried out on the surface tension driven Bénard convection prior to 2001, the reader is referred to the review of Schatz and Neitzel [1]. More recently, other studies were carried out to go deeper into understanding this flow and to further investigate the problems listed above [2 – 4]. Recently, books dealing with surface tensio-driven instabilities and interfacial phenomena were also published [5, 6].

As far as we know, no experimental study has been carried out to consider the influence of the thermal conductivity of the upper gas (Biot number) and the thermophysical properties of the fluid (Prandtl number) on the pattern formation and dynamics. The importance of the Biot number in the Thermocapillary convection has been recalled recently by Bok-Cheol and Zebib [7]. Indeed, Bénard - Marangoni experiments were most frequently performed with air as the upper gas layer (low Biot number) because it allows to simplify the theoretical modelling by permitting the density and the viscosity of the gas layer to be neglected. Consequently this paper deals with such problems using experimental techniques, by interferometry to visualize the free surface deformation fields and infrared thermography to visualize the interfacial temperature fields.

The outline of this paper is the following. The experimental set-up and procedure are described in section 2. Some results are presented in section 3. In section 4, conclusions are given.

2. Experimental procedure

The experimental set-up, as shown in Figure 1, consisted of a horizontal layer of silicone oil (with a depth of 2 mm or 5 mm). Various silicone oils were used (20 centistokes silicone oil with Prandtl number $Pr = \nu/\kappa = 206$ at 25°C, 50 centistokes silicone oil with $Pr = 474$ at 25 °C, and 100 centistokes silicone oil with $Pr = 935$ at 25 °C) set in a container with a flat bottom, which is made of copper, and lateral walls, which are made of polycarbonate. The fact that the polycarbonate has about the same thermal conductivity ($\lambda = 0.260$ W/m×K) as the silicone oil ($\lambda = 0.15$ W/m×K) reduces the heat leaks. The gas layer, above the oil layer, was made as thin as possible in order to suppress gas disturbances. A gas gap of 2 or 5 mm depth was used. Two cases were considered. An insulating upper layer (air with Biot number $L = \lambda_g d_l/\lambda_l d_g = 0.43$) and a conducting upper gas (helium with $L = 2.52$ for $d_l = 5$ mm and $d_g = 2$ mm, and $L = 0.4$ for $d_l = 2$ mm and $d_g = 5$ mm), where λ_l is the thermal conductivity of the silicone oil, λ_g is the thermal conductivity of the gas, and d_l and d_g are the depths of the liquid layer and the gas respectively. A single-crystal sapphire window of 3-mm thickness and 100-mm diameter, with top and bottom surfaces polished and optically flat, contained the gas. The purpose of the sapphire is to provide a transparent lid with a good thermal conductivity (41.900 W/m×K according to the manufacturer) which allows infrared measurements. The thermal conductivity of the sapphire is about 300 times larger than the thermal conductivity of the silicone oil. The uniform temperature of the sapphire combined with the small gas gap made the temperature of the gas on top of the silicone oil practically uniform, as required.

The vertical temperature gradient is applied by cooling the sapphire window and by a controlled heating of the lower plate, using Peltier elements. The bottom temperature fluctuated by less than ± 0.1 °C. The confinement of the fluid layer is taken into account by means of a non-dimensional parameter, the aspect ratio Γ, which is the ratio of a characteristic horizontal length (the radius of the container R = 30 mm) to the liquid depth, d_l. Experiments were performed in a circular vessel with $\Gamma = R/d_l = 6$ (for $d_l = 5$ mm) or $\Gamma = 15$ (for $d_l = 2$ mm). The liquid depth (d_l), was measured by means of a micrometer, with a precision of ± 0.05 mm. The possibilities of non-uniformity in the surface temperatures of both the top and bottom plates were checked with infrared thermography, and no horizontal temperature gradients were detected.

Flow visualization was achieved by interferometry (with a minimal detectable free surface deformation of ≈ 0.3 μm over a 60-mm diameter measurement area), and by thermography, a temperature field was obtained from the infrared radiation emitted by the oil-gas interface. Images of the convection patterns were recorded at regular time intervals. The images were digitized, and appropriate software allowed us to obtain the values of the relevant functions.
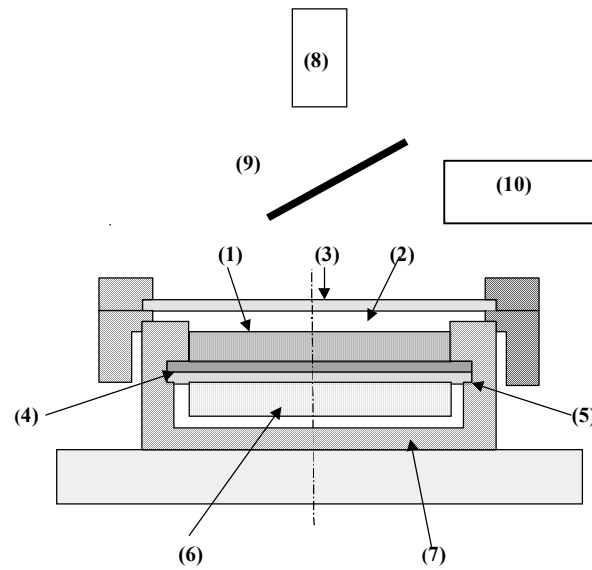
Figure 1. Schematic diagram of the experimental set-up. (1) Silicone oil layer, (2) gas layer, (3) sapphire window,(4) lower plate made of copper, (5) graphite plate,(6) Peltier element, (7) sidewalls made of polycarbonate, (8) interferometer, (9) mirror, (10) thermography camera.

Figure 2 represents an interfacial temperature field obtained by infrared thermography. Figure 3 shows an example of a free surface deformation field obtained by interferometry. Figure 4 is a 3-D representation obtained by transforming the intensity of each pixel of the original image of Figure 3 to an elevation. The two techniques are complementary. The thermography allows visualization of the entire pattern. Indeed, Figure 2 shows the peripheral cells, whereas in Figure 3, these cells cannot be visualized due to the fact that the interferometry cannot be used in the region with a meniscus. On the other hand, interferometry allows measuring the upper free surface deformation, which is an important parameter in BM convection.
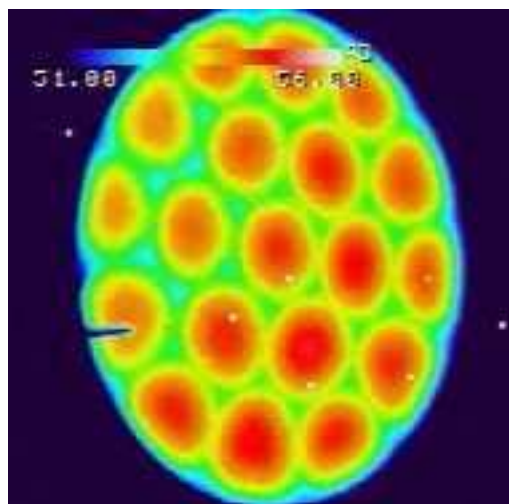
Figure 2. Example of a temperature field obtained by infrared thermography in a cylindrical vessel.
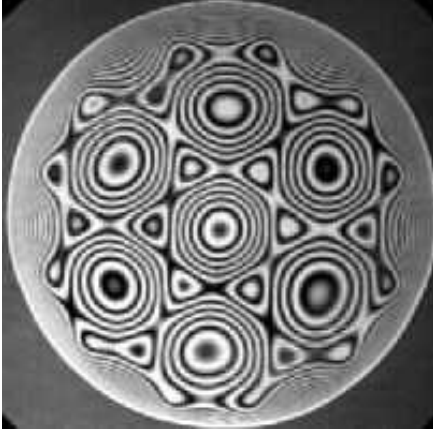
Figure 3. Example of a pattern, visualized by interferometry.
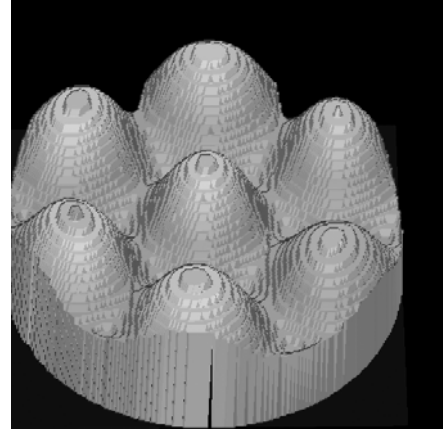
Figure 4. 3-D representation of the free surface deformation field.

The actual temperature difference applied to the fluid has to be calculated from the temperature difference between the lower plate and the temperature of the sapphire because no temperature sensor can be set in the narrow gas gap or on the fluid upper surface itself without introducing a disturbance.

The temperature difference across the fluid follows from the formula, assuming conductive heat transport,

$$\Delta T = \frac{\Delta T_p}{\left(1 + \dfrac{\lambda_l d_g}{\lambda_g d_l}\right)} = \frac{\Delta T_p}{\left(1 + \dfrac{1}{L}\right)} \tag{1}$$

where ΔT_p is the temperature difference between the sapphire and the lower copper plate and L is the Biot number. λ_l is the thermal conductivity of the silicone oil, λ_g is the thermal conductivity of the gas, and d_l and d_g are the depths of the liquid layer and the gas respectively.

The temperature difference applied to the fluid layer can be expressed in non dimensional form by the Marangoni number:

$$Ma = \left(-\frac{d\sigma}{dT}\right)\frac{\Delta T\, d_l}{\rho\nu\kappa} \tag{2}$$

and the Rayleigh number:

$$Ra = \frac{\alpha g \Delta T\, d_l^3}{\nu\kappa} \tag{3}$$

where $d\sigma/dT$ is the variation of the surface tension coefficient, σ, with temperature, ΔT the temperature difference applied to the liquid layer, ρ the density of the liquid, ν the kinematic viscosity, κ the thermal diffusivity, and α the expansion coefficient of the silicone oil, with g being the acceleration due to gravity.
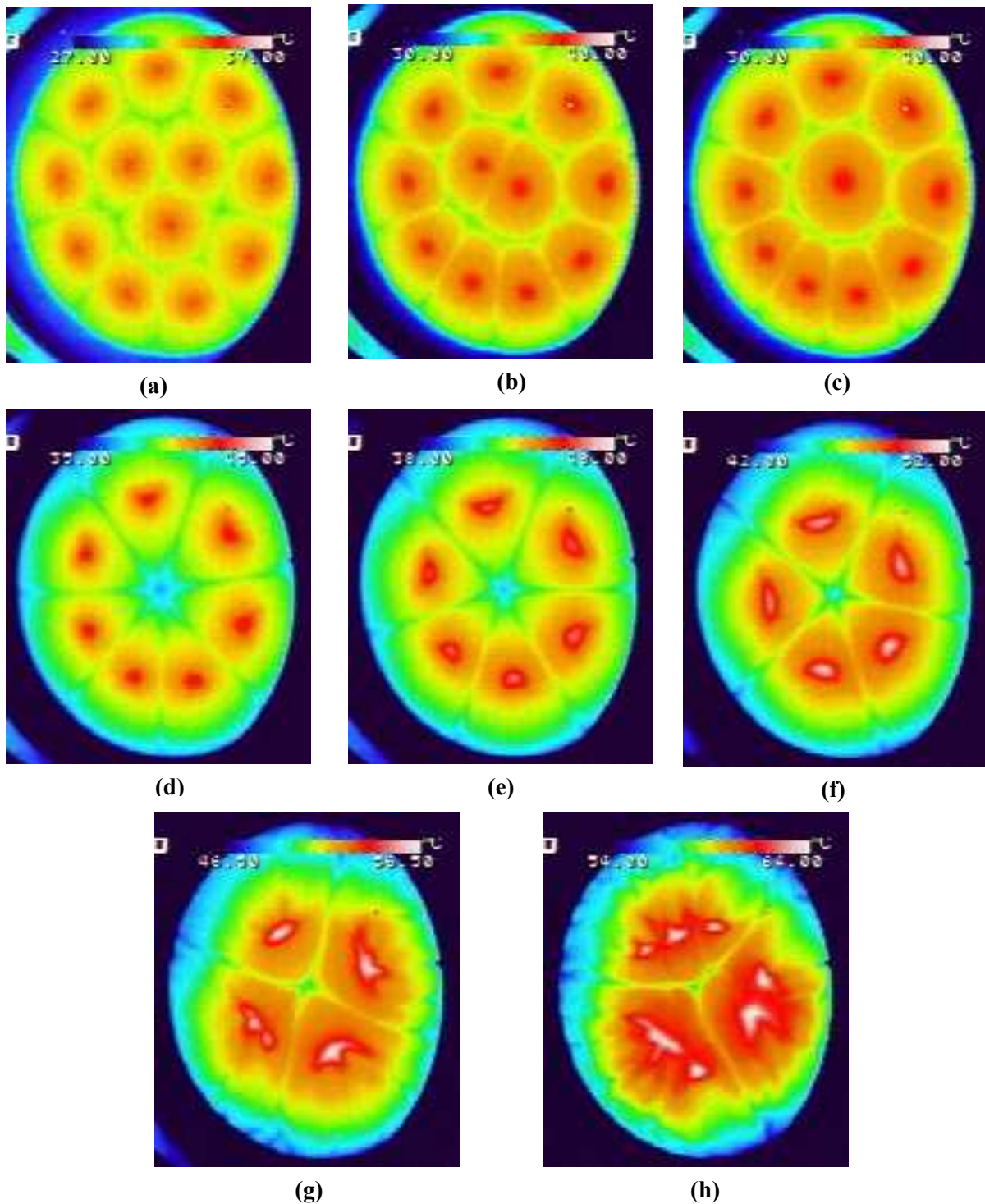
Figure 5. Patterns visualized by infrared thermography for various experimental conditions in a cylindrical vessel

$\Gamma = 6$, $L = 2.52$, $Pr = 206$, $\Delta T_p = $ (a) 10 °C, (b) between 10 °C and 15 °C, (c) 15 °C, (d) 20 °C, (e) 25 °C, (f) 30 °C, (g) 35 °C, (h) 45 °C.

3. Results and discussion

3.1. Temperature fields and pattern dynamics

Interfacial temperature fields obtained by infrared thermography and showing a typical sequence of transitions between patterns is given in Figure 5. During this experiment with a 5 mm layer, Pr = 206 and L = 2.52, pattern dynamics were observed, when the difference of temperature (ΔT_p) was increased from $\Delta T_p = 10$ °C to 50 °C.

After the onset of convection, a pattern with 3 central cells and 9 peripheral cells (cells in contact with the sidewall), is observed (Figure 5(a)). Between $\Delta T_p = 10$ °C and 15 °C, only 2 cells remain in the central part of the container (Figure 5(b)). For $\Delta T_p = 15$ °C, there is a pattern formed of one cell surrounded by 9 peripheral cells (Figure 5(c)). When ΔT_p is increased from 15 °C to 20 °C, the sizes of the peripheral cells increase and these cells expand towards the center of the container inducing the disappearance of the central cell (Figure 5(d)). After that, there is a transition to a pattern formed of 6 cells for $\Delta T_p = 25$ °C (Figure 5(e)). A structure with 5 cells is observed for $\Delta T_p = 30$ °C (Figure 5(f)) and a pattern formed of 4 cells for $\Delta T_p = 35$ °C (Figure 5(g)). During the increase of ΔT_p from 40 °C to 50 °C, a pattern with 3 cells is observed and in each cell, the flow behaves in a complex manner with oscillating hot spots indicating the transition to time dependent flow (Figure 5(h)).

For Pr = 206 and L = 0.43, we observed almost the same sequence as above but larger ΔT_p were needed to observe the transitions between the various patterns, for example the pattern with 3 central cells and 9 peripheral cells was observed for $\Delta T_p = 15$ °C, the pattern with 4 cells was observed for $\Delta T_p = 50$ °C.

For Pr = 474 and L = 2.52, $\Delta T_p = 35$ °C is needed to observe a pattern with one central cell and 9 peripheral cells and $\Delta T_p = 50$ °C had to be applied to observe a pattern with 7 cells.

For Pr = 935 and L = 2.52, we observed only one pattern formed of 4 central cells and 9 peripheral cells for $\Delta T_p = 5$-50 °C.

For Pr = 935 and L = 0.43, for $\Delta T_p = 5$-50 °C, the only pattern observed is that composed of 3 cells surrounded by 10 peripheral cells.

For Pr = 206 and Pr = 474, when the Biot number is increased from L = 0.43 to L = 2.52, more dynamics are observed and smaller gradients of temperature are needed to reach the onsets of the various instabilities and transitions between patterns.

On the other hand, when the Pr number is increased, less dynamics are observed and the gradients of temperature necessary to observe the transitions between the various states of the flow are larger. For Pr = 935, it seems that the influence of ΔT_p and L on the dynamics is negligible (at least in the limits of the studied experimental range)>, that means that the viscous effects are so important that the pattern does not react to the increase of the heat transfer rate at the oil-gas interface obtained by the use of a more conductive gas (helium instead of air).

The total number of cells (N_c) decreases (the cell size increases) as a function of ΔT_p (Figure 6). As expected, the number of cells increases as Γ is increased, indeed there are more cells for the larger aspect ratio ($\Gamma = 15$ corresponding to the thinner layer, $d_l = 2$ mm) than for the smaller one ($\Gamma = 6$ corresponding to the 5-mm oil layer) (Figure 6). The behaviour of (N_c) as a function of the applied gradient of temperature confirms the results obtained in [8, 9].

The total number of cells is larger for higher Pr (= 474) than for the lower value (Pr = 206), as it can be seen in Figure 6. As for the variation as a function of the Biot number, the total number of cells decreases as a function of ΔT_p, and there are more cells for lower L (= 0.43) than for the larger Biot number (L = 2.52).
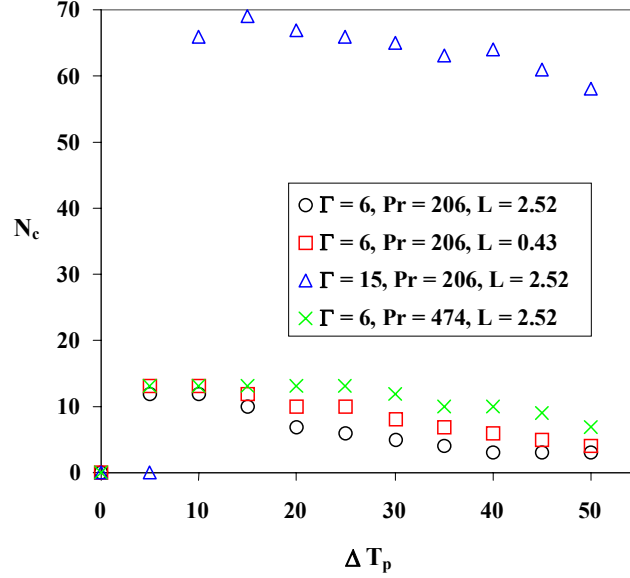
Figure 6 .The total number of cells (N_c) as a function of ΔT_p, for various experimental conditions.

3.2. Free surface deformation fields

The interferometry technique allows to visualize the patterns and also to measure the upper free surface deformation magnitude. For d_l = 5 mm, according to Cerisier et al. [10], the buoyancy effects are preponderant and the deformation of the upper free surface is convex. Figure 7 shows three patterns corresponding to various gradients of temperature. It can be clearly seen that when ΔT_p increases more fringes are observed which means that the magnitude of the deformation increases with ΔT_p.

In Figure 8, the upper free surface deformation magnitude, for a convection cell visualized by interferometry, as a function of ΔT_p is shown for various experimental conditions. It can be seen that it increases as a function of ΔT_p for all the experimental conditions.

Cerisier et al. [10] also found that the magnitude of the deformation increases with the applied gradient of temperature. In Figure 8, there are two behaviours depending on the value of ΔT_p. For ΔT_p < 20 °C and for a same ΔT_p, the deformation is larger for L = 2.52 than for L = 0.43 and is larger for lower Pr number (= 474) than for the higher Pr number (= 935). For ΔT = 20 °C, the same deformation is observed for all the experimental conditions. Beyond ΔT_p = 20 °C, the inverse behaviour is observed, for a same ΔT_p, the deformation magnitude is larger for the lower L than for the higher L and we observe more deformation at higher Pr than for lower Pr.

The behaviour as a function of L, for ΔT_p > 20 °C, may be explained by the fact that when the rate of heat transfer from the upper surface is increased, the normal and the tangential temperature gradients are not proportionally increased which results in reduced temperature gradients along the surface and therefore reduced surface tension gradients. Temperature gradients normal to the surface, however, are increased by the larger heat transfer at the surface producing increased density gradients in the bulk of the liquid. Since buoyancy forces increase and surface tension forces decrease with

enhanced heat transfer rate, increasing the rate of surface cooling (by increasing the Biot number) may reduce the magnitude of the surface deformation.

(a)

(b)

(c)
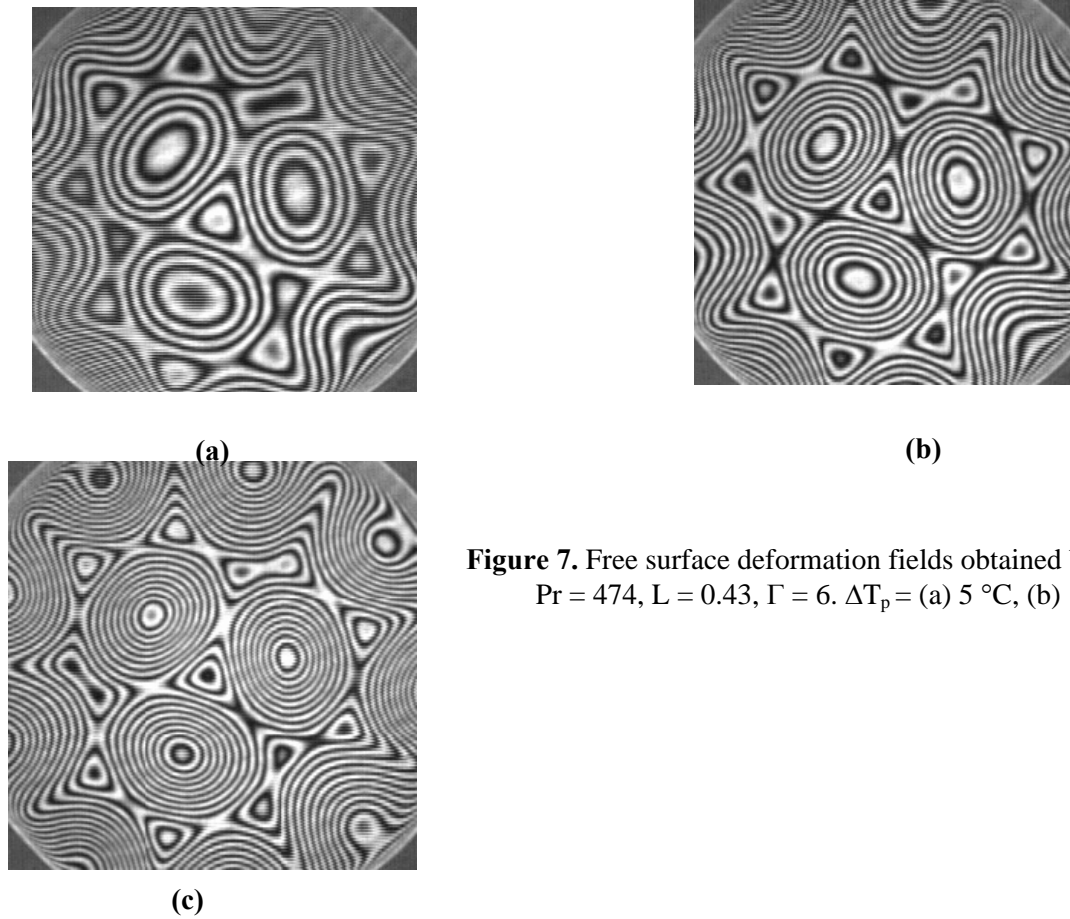
Figure 7. Free surface deformation fields obtained by interferometry. Pr = 474, L = 0.43, Γ = 6. ΔT_p = (a) 5 °C, (b) 15 °C, (c) 25 °C.

Deformation magnitude (μm)

○ **Pr = 935, L = 2.52**
□ **Pr = 935, L = 0.43**
△ **Pr = 474, L = 0.43**

ΔT_p (°C)
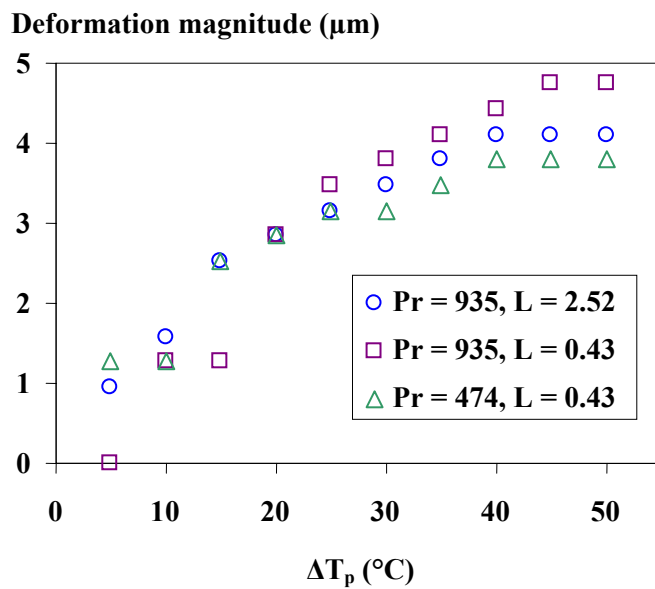
Figure 8. The upper free-surface deformation magnitude as a function of the applied gradient of temperature (ΔT_p), for various experimental conditions. (Γ = 6).

4. Conclusions

In this paper, we studied the influence of various physical parameters (ΔT, Pr number, aspect ratio, and Biot number) on the formation and dynamics of patterns involved in the BM convection in small to medium aspect ratios.

This study was made possible by the measurements of free surface deformation and temperature fields. These two techniques are complementary, since each method provides specific information, which may allow the detection of peculiar phenomena such as the spatial resonance, which is a situation in which the interfacial deformation does not conform to the pattern flow [11].

Previous results of other authors were confirmed concerning the evolution as functions of the applied gradient of temperature and new results were obtained concerning the behaviour of the pattern as functions of Pr and Biot numbers. Increasing the Biot number was found to induce more dynamics of the pattern particularly for Pr = 206 and Pr = 474. Increasing the Prandtl number reduces the pattern dynamics.

The upper free surface deformation and the wavenumber increase as functions of the applied gradient of temperature. Two behaviours of the deformation, depending on the value of the gradient of temperature, were observed, as functions of the Prandtl and Biot numbers.

References

[1] Schatz M F and Neitzel G P 2001 Experiments on thermocapillary instabilities *Ann. Rev. Fluid Mech.* **33(6)** 93 - 127.

[2] Cerisier P, Billia B and Rahal S 2001 Evolution and stability limits of patterns in surface-tension-driven Bénard convection *Journal of Non-Equilibrium Thermodynamics* **26 (02)** 99 - 118.

[3] Colinet P, Nepomnyashchy A A and Legros J C 2002 Multiplication of defects in hexagonal patterns *Europhys. Lett.* **57** 480 - 86.

[4] Young Y and Riecke H 2002 Mean flow in hexagonal convection: stability and nonlinear dynamics *Physica* D **163** 166 - 183.

[5] Colinet P, Legros J C and Velarde M G 2001 *Nonlinear dynamics of surface-tension-driven instabilities* (Berlin: Wiley-VCH).

[6] Nepomnyashchy A A, Velarde M G and Colinet P 2002 *Interfacial phenomena and convection* (Chapman & Hall/CRC, Boca Raton).

[7] Bok-Cheol S and Zebib A 2002 Effect of free surface heat loss and rotation on transition to oscillatory thermocapillary convection *Physics of Fluids* **14(1)** 225 - 31.

[8] Cerisier P, Perez-Garcia C, Jamond C and Pantaloni J 1987 Wavelength selection in Bénard Marangoni convection *Phys. Rev.* A **35** 1949 -52.

[9] Koschmieder E L and Switzer D W 1992 The wavenumbers of supercritical surface-tension-driven Benard convection *J. Fluid Mech.* **240** 533 - 48.

[10] Cerisier P, Jamond C, Pantaloni J and Charmet J C 1984 Déformation de la surface libre en convection de Bénard-Marangoni *J. Physique* **45** 405 - 11.

[11] Hadji L 1996 Non linear analysis of the coupling between interface deflection and hexagonal patterns in Rayleigh-Benard-Marangoni convection *Phys. Rev.* E **53** 5982 - 92.